Cytometry
PART A
Journal of the International Society for Advancement of Cytometry

Super-Resolved Calibration-Free Flow Cytometric Characterization of Platelets and Cell-Derived Microparticles in Platelet-Rich Plasma

Anastasiya I. Konokhova,[1] Darya N. Chernova,[1,2] Alexander E. Moskalensky,[1,2] Dmitry I. Strokotov,[1,3] Maxim A. Yurkin,[1,2] Andrei V. Chernyshev,[1,2] Valeri P. Maltsev[1,2,3]*

[1]Institute of Chemical Kinetics and Combustion SB RAS, 630090 Novosibirsk, Russia

[2]Novosibirsk State University, 630090 Novosibirsk, Russia

[3]Novosibirsk State Medical University, 630091 Novosibirsk, Russia

Received 19 August 2014; Revised 13 November 2014; Accepted 12 December 2014

Grant sponsor: Russian Science Foundation (The experimental work with platelets); Grant number: 14-15-00155; Grant sponsor: Russian Foundation for Basic Research (The experimental work with microparticles); Grant number: 12-04-00737-a; Grant sponsor: Stipend of the President of Russian Federation for Young Scientists (to M.A.Y, A.E.M, D.I.S).

Correspondence to: Valeri P. Maltsev; Institute of Chemical Kinetics and Combustion SB RAS, Institutskaya 3, 630090 Novosibirsk, Russia.
E-mail: maltsev@kinetics.nsc.ru

Published online 00 Month 2015 in Wiley Online Library (wileyonlinelibrary.com)

DOI: 10.1002/cyto.a.22621

Abstract

Importance of microparticles (MPs), also regarded as extracellular vesicles, in many physiological processes and clinical conditions motivates one to use the most informative and precise methods for their characterization. Methods based on individual particle analysis provide statistically reliable distributions of MP population over characteristics. Although flow cytometry is one of the most powerful technologies of this type, the standard forward-versus-side-scattering plots of MPs and platelets (PLTs) overlap considerably because of similarity of their morphological characteristics. Moreover, ordinary flow cytometry is not capable of measurement of size and refractive index (RI) of MPs. In this study, we 1) employed the potential of the scanning flow cytometer (SFC) for identification and characterization of MPs from light scattering; 2) suggested the reference method to characterize MP morphology (size and RI) with high precision; and 3) determined the lowest size of a MP that can be characterized from light scattering with the SFC. We equipped the SFC with 405 and 488 nm lasers to measure the light-scattering profiles and side scattering from MPs, respectively. The developed two-stage method allowed accurate separation of PLTs and MPs in platelet-rich plasma. We used two optical models for MPs, a sphere and a bisphere, in the solution of the inverse light-scattering problem. This solution provides unprecedented precision in determination of size and RI of individual spherical MPs—median uncertainties (standard deviations) were 6 nm and 0.003, respectively. The developed method provides instrument-independent quantitative information on MPs, which can be used in studies of various factors affecting MP population.

Key terms

flow cytometry; microparticles; platelets; light scattering; refractive index; vesicles; inverse light-scattering problem

Microparticles (MPs) are plasma membrane-derived vesicles, released from cells during stress conditions, including activation and apoptosis (1). MPs are present in peripheral blood and body fluids and constitute a heterogeneous population of particles highly variable in size, composition, concentration, cellular origin, and functional properties (2). MPs are involved in many physiological processes, including intracellular communication and crosstalk, homeostasis and pathogenesis, inflammation and coagulation, and may be potentially useful as diagnostic or prognostic biomarkers and pathogenic agents (3–6). The clinical importance of MPs has been recognized, but validating of MP diagnostic potential and direct application of MP analysis in clinical practice is hampered due to the absence of standardized methods for MP identification and characterization.

ISAC
International Society for Advancement of Cytometry

The size of MPs is typically defined in ranges between 100 nm and 1 μm, but experimentally determined ranges widely vary between studies. This variance might be explained by limitations of the methods applied for the detection and characterization of MPs and differences in MP isolation protocols, including centrifugation speed, filtration conditions, and sample storage (7,8). Centrifugation is a crucial step in processing blood samples for MP analysis, which is used to increase relative concentration of MP during analysis and prevent the formation of new MPs from parent cells. However, even single centrifugation (1,500*g* for 20 min, i.e., 30,000*g*·min) used to obtain platelet-poor plasma from whole blood not only removes most platelets (PLTs), but also results in loss of variable number of MPs (9). Moreover, such procedure may also lead to underestimation of some of MP functional properties, related to size, such as procoagulant phospholipid activity (10). As the analysis of MP in the whole blood samples is complicated due to a relatively small MP concentration, the preferable delicate way to measure MPs is to remove red blood cells by soft centrifugation (about 1,000*g*·min) and to analyze the platelet-rich plasma (PRP). From the one hand, the presence of PLTs in PRP may be considered as a disadvantage due to continuous in vitro formation of platelet-derived MPs that requires immediate processing of the PRP samples (9). From the other hand, the removal of PLTs from PRP by filtration instead of further centrifugation is also objectionable, as it may lead to PLT activation, fragmentation, and unexpected increase in total MP number (8,11). The presence of PLTs in PRP provides an opportunity of their simultaneous characterization. Such a comprehensive analysis seems to be more natural with the majority of MPs originating from PLTs (12). The major problem in this approach, however, is that smaller PLTs are morphologically similar to the larger MPs and MP aggregates, which complicates their separation (13).

The characterization means determination of physical characteristics of analyzed particles, like volume, shape, density, and internal structure. A reference method should provide the highest precision in determination of particle characteristics and be instrument-independent, so that different research groups could compare their results. Precise determination of the distributions over MP characteristics should allow one to observe its changes during different physiological processes, like apoptosis and PLT activation, or any other variations of blood environment. The accurate measurement of MP size guarantees a high sensitivity of the distribution parameters to effects of these processes. However, to reach the nanometer precision in measurement of MP size, one has to take into account the other MP characteristics which affect experimental signals. For instance, scattering amplitudes in flow cytometry (14) and diffraction pattern in multiangle measurements (15) depend on the refractive index (RI) and shape of scatterers. The shape of a particle, its membrane ion conductivity, and the cell trajectory within an orifice take effect on impedance-based measurements (16,17). These other MP characteristics have to be determined simultaneously with the size measurement or be reliably estimated independently.

The particle analysis can be performed either on individual particles sequentially or on a large population of particles at once. For example, the multiangle light-scattering method, implemented in a laser diffraction particle size analyzer is based on the measurement of light scattering from particle suspensions and has substantial fundamental limitations in inversion of a size distribution without a priori information (15). The dynamic light scattering method is potentially suitable for analysis of MPs and PLTs in PRP (18,19), but it also requires a priori information, in particular, about the sample monodispersity (20). Alternatively, an instrument based on single-particle analysis generally leads to better precision of the particle characteristics because it utilizes only an optical model of a single particle but assumes nothing about the size distribution. The requirement of measurement MPs in PRP significantly narrows a variety of available methods, which are already limited by small sizes of MP and high heterogeneity over their characteristics. The reviews (21,22) summarize the capabilities of both optical and nonoptical methods for MP characterization and leave the following options: scattering flow cytometry, nanoparticle tracking analysis, impedance-based flow cytometry, optical microscopy, transmission electron microscopy, and atomic force microscopy. Evidently, transmission electron microscopy and atomic force microscopy could not be a base of the reference method for MP characterization because of low statistical relevance and laborious sample preparation. Optical microscopy has a low spatial resolution to characterize MPs. Impedance-based flow cytometry with measurement of the forward (FSC), side (SSC) scattering, and amplitude of the current pulse when a MP flows through of the orifice, requires one to solve the ill-posed problem resulting in substantial errors in characteristic estimates. The three measured numbers depend on the size, shape, RI, ion membrane conductivity, and MP trajectory within the orifice. Moreover, the small size of the MPs leads to orifice with a diameter less than 20 μm that is susceptible to clogging. The nanoparticle tracking analysis measures only the hydrodynamic size of individual nanoparticles (23), although estimation of the particle RI from the intensity of the scattered light has been demonstrated (24). The main issue, however, is the undefined uncertainties of single measurements for both size and RI.

The flow cytometry still remains the most widely applied method to detect MPs in clinical samples (25). However, in ordinary configuration (FSC and SSC), it does not provide identification of MPs/PLTs because of similarity of morphological characteristics of MPs, MP aggregates, and PLTs. Moreover, the characterization of MPs/PLTs could neither be carried out with ordinary flow cytometer because of insufficient experimental data. The FSC and SSC depend on shape, size, RI of the measured particles, and instrumental geometry of flow cytometers including collecting optics and beamstops. Many efforts are aimed at standardization of MPs measurements by flow cytometry for proper MP identification including sample preparation, immunostaining, and particle size-calibration protocols (9,11,22,25). But even the determination of the relationship between the measured light-

scattering intensity (FSC or SSC) and the diameter of studied particles led to contradictions between measurement results obtained on different instruments due to differences in their optical configurations (13,26,27). In addition, the procedure of size calibration for converting measured scattering signals into particle size requires some assumptions on RIs of measured particles, which actually may vary in wide ranges, and sphericity of their shape (cf. MP aggregates). Moreover, the scattering signal exceeding the threshold does not necessarily correspond to the single detected particle but also can be related to background particles, optical and electronic noise, or to coincident detection of multiple small particles (28,29). There are also insufficient experimental data to estimate the errors of characteristic estimates. The same problems are relevant to characterization of PLTs in contrast to MPs possess more complicated shape and scattering properties (30).

In our previous study (31), we developed a method to identify and characterize MPs with the scanning flow cytometer (SFC), which measures angle-resolved light-scattering profiles (LSPs) of individual MPs. This method allows one to identify spherical MPs in blood plasma, unambiguously separating them from other plasma particles, optical and electronic noise, and coincident detection events, without MP staining and polystyrene bead gating procedure, and to characterize individual MPs by their size and RI through the solution of the inverse light-scattering (ILS) problem. However, the uncertainties in determined MP characteristics were so large that no details of the corresponding distributions could be analyzed. Moreover, only the MPs with a size larger than 500 nm could be detected due to the used laser with a wavelength of 660 nm.

In this study, we report a new method for simultaneous identification and characterization of MPs and PLTs in PRP, improving MP characterization method and combining it with our previously developed method to measure PLTs volume and shape (30). The accuracy of MP characterization was improved by 1) replacement of the 660 nm laser by the 405 nm one for LSP measurement, 2) usage of the SSC amplitude as an additional light-scattering data in the solution of the ILS problem for spherical particles, and 3) usage of two optical models, a sphere and a bisphere, to describe MPs shape and, hence, to identify single MPs and MP aggregates. This allowed us to reduce the threshold in detection of MPs, to enhance the identification power of the MPs from light scattering in PRP, and to decrease largely the uncertainties of MP size and RI. Additionally, the developed approach allowed us to determine simultaneously volume of PLTs, thus increasing the diagnostic and research significance of the method.

Materials and Methods

Sample Preparation

After written informed consent, the whole blood sample were obtained from a healthy volunteer by venipuncture, collected in a vacuum tube (BD Vacutainer Systems, BD, UK) containing ethylenediaminetetraacetic acid as anticoagulant, and processed within 2 h of being obtained. Isolation of MP

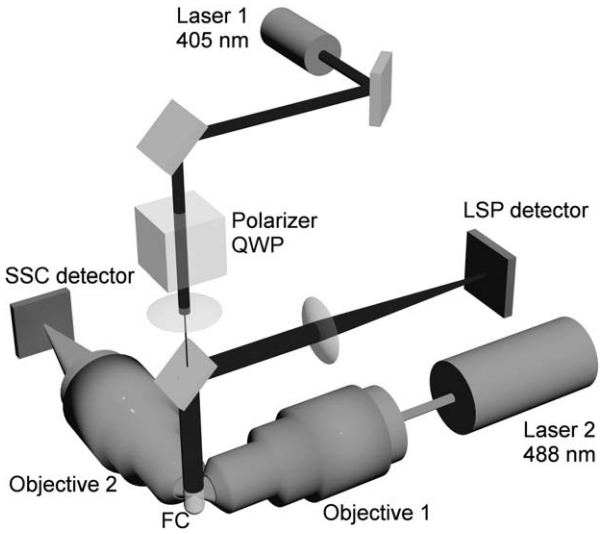

Figure 1. SFC optical setup. LSP detector, light-scattering profile detector; SSC detector, side-scattering detector; FC, flow cell; QWP, quarter-wave plate.

was realized with continuously prepared two samples: the first sample (untreated PRP) contained the plasma supernatant formed in a tube with a whole blood sample within 2 h of the collection and the second sample (centrifuged PRP) contained supernatant formed in a tube with whole blood centrifuged at 200*g* for 10 min (2,000*g*·min). To test the sensitivity of MP characterization, we prepared the third sample (filtered PRP) additionally filtering the centrifuged PRP through 1.2-μm filter (Sartorius AG, Stedim Biotech GmbH, Goettingen, Germany). Finally, we added 1-μm polystyrene microspheres (Molecular Probes, Eugene, OR) to each sample as a reference. The samples were diluted by 200-, 100-, and 50-fold, respectively, in 0.2 μm filtered (Sartorius Stedim Biotech GmbH, Goettingen, Germany) 0.9% saline. We also measured 0.4-μm polystyrene beads (Molecular Probes, Eugene, OR) to analyze its applicability for gating MP events by FSC as it was proposed and done by Chandler et al. (13).

Need to note that analysis with SFC does not require us to use the bead size from manufacturer specifications. LSPs measured with the SFC and solution of the ILS problem provide direct determination of a size of individual beads.

Scanning Flow Cytometer

To determine particle characteristics from light scattering, we used the following workflow: light-scattering measurement → particle identification → optical model of the particle → theoretical simulation of light scattering → solution of the ILS problem. The light-scattering measurements of individual particles were performed with the SFC, which allows one to measure LSPs of individual particles (32). Technical features of the SFC and the operational function of the optical cell were described in detail elsewhere (33,34). The actual SFC was fabricated by Cytonova Company (Novosibirsk, Russia). Here, we briefly describe the schematic optical layout of the SFC shown in Figure 1. The part of the SFC formed by Laser 2

(488 nm, 15 mW, FCD488-020, JDS Uniphase Corporation, Milpitas, CA), Objective 1 (NA = 0.1), flow cell (FC), Objective 2 (NA = 0.5), and SSC detector (photomultiplier tube, H9 305-04, Hamamatsu, Shizuoka Pref., 430-8587, Japan) is identical to that of an ordinary flow cytometer. The polarization of Laser 2 was orthogonal to the scatter plane formed by Objective 1 and Objective 2. The SSC detector generates SSC signal to be used in the solution of the ILS problem for spherical particles and to trigger the electronics of the SFC. The other part formed by Laser 1 (405 nm, 30 mW, Radius, Coherent, Santa Clara, CA), Polarizer, quarter-wave plate (QWP), FC, and LSP detector (photomultiplier tube, H9 305-04, Hamamatsu, Shizuoka Pref., 430-8587, Japan) generates the LSP of individual particles carried by the flow.

Within the formalism of the Mueller scattering matrix S (35), the intensities measured by LSP and SSC detectors are the following (34):

$$I_{\text{th}}^{\text{LSP}}(\theta) = k_1 \int_0^{2\pi} [S_{11}(\theta,\varphi) + S_{14}(\theta,\varphi)]d\varphi, \quad (1)$$

$$I_{\text{th}}^{\text{SSC}} = k_2 \int\int_{\text{apert.}} d\theta d\varphi \sin\theta [S_{11}(\theta,\varphi) - S_{12}(\theta,\varphi)\cos(2\varphi) - S_{13}(\theta,\varphi)\sin(2\varphi)], \quad (2)$$

where θ and φ are the polar and azimuthal scattering angles, k_1 and k_2 are the scaling coefficients determined from the measurement of reference 1-μm polystyrene microspheres. The "apert." in Eq. (2) is the circular aperture of the Objective 2 (Fig. 1) with a center of 90° for both θ and φ and NA = 0.5. The operational LSP polar angle range of the SFC was determined from analysis of 1-μm polystyrene microspheres, as described by Strokotov et al. (36), to be from 5° to 70°. All experimental and theoretical LSPs presented in this study are additionally multiplied with the weighting function:

$$w(\theta) = \frac{1^\circ}{\theta} \exp\left(-2\ln^2(\theta/54^\circ)\right), \quad (3)$$

which is an approximation of the SFC transfer function and provides an uniform experimental-noise level over the considered angular region (33). The detection threshold of the described SFC is primarily determined by the SSC amplitude. However, the SFC has exceptional S/N ratio for the LSP signal due to the increased diaphragm of the LSP detector, collection of the scattered light over the whole azimuthal angle, and use of the laser with a shortest visible wavelength of 405 nm. This leads to small characterization uncertainties, which are further decreased by discarding particles with S/N ratio of measured LSPs less than 2. Thus, we miss a number of potentially detectable smaller particles, but keep the reliability of extracted particle characteristics.

Platelet and MP Identification in PRP. We utilized the two-stage algorithm for identification of cells in PRP. At the first stage, we applied the database of PLT LSPs, previously computed with the discrete dipole approximation (30,37) to process the untreated PRP, which allowed us to determine equivolume diameters (diameter of the sphere with the same volume, d_{ev}) of PLTs with subdiffraction precision (30). We constructed the FSC (which is LSP intensity integrated from 5° to 10°) versus d_{ev} map for particles from the untreated PRP. The PLT gate was set as a 99% elliptic confidence region (three standard deviations), defined by covariance matrix, robustly estimated over all plotted points using Minimum Covariance Determinant estimator (38) implemented in package RRCOV (39). In the second stage, we employed this gate to remove PLTs from centrifuged and filtered PRP. The rest are assumed to be non-PLT plasma particles, including MPs, to be identified and characterized with the subsequent solution of the ILS problem.

Optical Models of MPs and Light-Scattering Simulations

The most obvious optical model of a MP is a sphere, but electron microscopy shows that not all MPs are spherical. In particular, analysis of the scanning and transmission electron micrographs [(40), Figs. 2 and (41) 1A, respectively] reveals MPs which can be modeled by a sphere, aggregate of spheres, prolate spheroid, cylinder, and so forth. However, some of these MPs may have not originated from in vivo conditions but have been formed by the sample preparation (40). Details of particle shape are especially important for subdiffraction resolution that we aim to achieve. Thus, we applied the following optical models: a sphere and a bisphere (aggregate of two spheres having equal RIs). The latter is the simplest approximation of aggregated MPs and is described by four characteristics (two diameters d_1 and d_2, RI n, and angle β between direction of light propagation and bisphere symmetry axis), while a sphere—only by two (diameter d and RI n). Finally, the bisphere size can also be described by equivolume diameter d_{ev} to be used along with actual diameter of the spherical model to characterize MP size. Here and further, we consider all RIs at wavelength of LSP (405 nm) unless noted otherwise.

It is important to note that a bisphere is a somewhat arbitrary chosen nonspherical shape as a first approximation to a wide variety of existing shapes other than simple spheres. We tried two other nonspherical models: spheroid and rods, and found that they are generally less capable to describe the nonspherical MP events, that is, they produce satisfactory fits for lesser fraction of events than that by bisphere model (data not shown). The detailed discussion of applicability of the bisphere model and of related caveats is given in Section "Results."

According to the chosen optical models of MPs, the following light-scattering theories were utilized in simulation: the Mie theory (35) for spheres and T-matrix method (42) for bispheres. The medium (0.9% saline) RI in simulations was assumed to be 1.345 and 1.339 at wavelengths of 405 and 488 nm, respectively, according to the dispersion formula for aqueous solutions (43).

ILS Problem

The ILS problem is transformed into the global minimization of the weighted sum of squares:

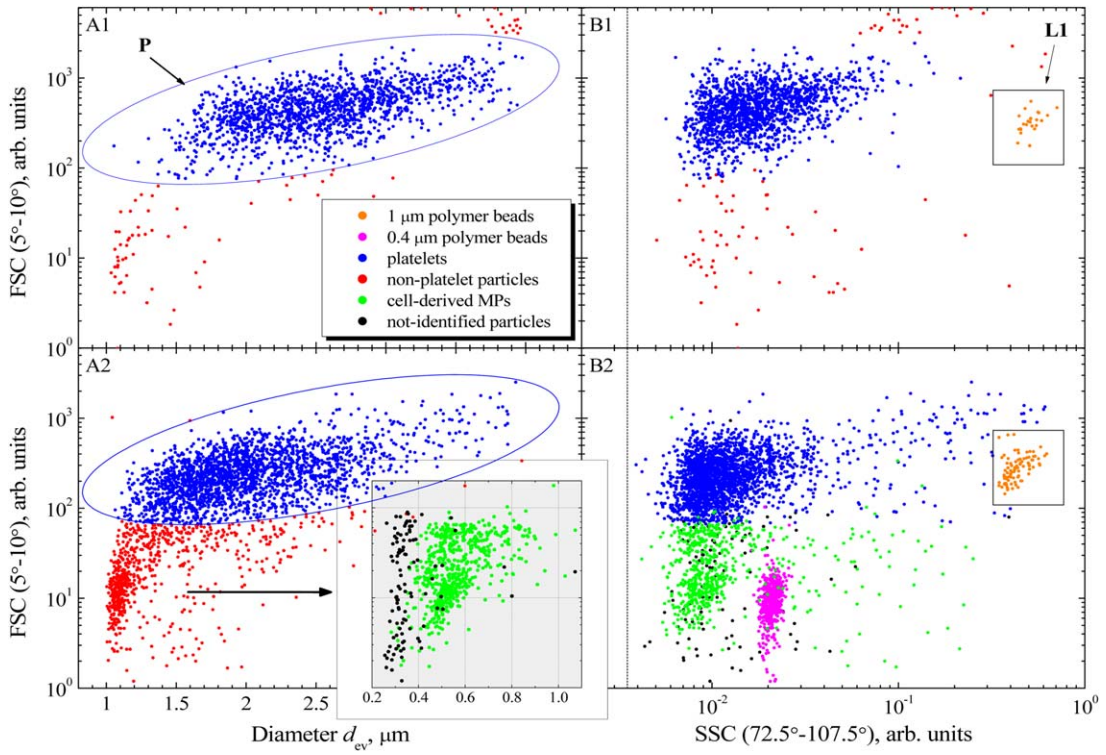

Figure 2. FSC versus equivolume diameter (**A1** and **A2**) and FSC versus SSC (**B1** and **B2**) maps of untreated PRP (A1 and B1) and centrifuged PRP at 2,000*g*·min (A2 and B2). The 1- and 0.4-μm polymer beads are shown for a reference. The dashed lines in column (B) show the threshold that triggers the flow cytometer electronic unit. Platelet gate (ellipse) determined from (A1) is used to isolate PLTs in (A2). Sizes of non-PLTs (red points) in the main part of (A2) are largely biased and are further determined by a completely different algorithm. The results of the latter (with realistic sizes) are given in the inset with separation into MPs (spherical or bisphere-like) and not-identified particles (unknown shapes).

$$S(\mathbf{P},\eta)=\sum_{i=1}^{N}[w(\theta_i)]^2\left[I_{\text{exp}}^{\text{LSP}}(\theta_i)-\eta I_{\text{th}}^{\text{LSP}}(\theta_i,\mathbf{P})\right]^2 \qquad (4)$$

where $\mathbf{P}$ is a vector of model characteristics ($\{d,n\}$ for spheres and $\{d_1,d_2,n,\beta\}$ for bispheres), N is a number of LSP points, $I_{\text{exp}}^{\text{LSP}}(\theta_i)$ is an experimental LSP, $I_{\text{th}}^{\text{LSP}}(\theta_i,\mathbf{P})$ and $w(\theta_i)$ are given by Eqs. (1), respectively, and coefficient η compensates the effect of the particle trajectory in the FC of the SFC. For spheres, we employed global optimization method DiRect (36,44) with characteristic bounds set as $d\in[0.1, 2]$ μm, $n\in[1.35, 1.7]$. Moreover, to improve the accuracy of the solution, we used extra light-scattering information from measured SSC signal as a constraint:

$$I_{\text{exp}}^{\text{SSC}}=I_{\text{th}}^{\text{SSC}}(\mathbf{P}), \qquad (5)$$

where $I_{\text{exp}}^{\text{SSC}}$ and $I_{\text{th}}^{\text{SSC}}(\mathbf{P})$ are the amplitudes of experimental and theoretical [Eq. (2)] SSC intensities, respectively. The SSC amplitude can be used only for spherical particles because $I_{\text{th}}^{\text{SSC}}(\mathbf{P})$ of nonspherical particles depends on additional (azimuthal) orientation angle, which does not affect the LSP.

It is also not feasible to apply direct fit to nonspherical particles due to much larger computational time required to simulate the LSP. Thus, we used the nearest-neighbor interpolation using the precalculated database of LSPs, which is described in details for PLTs in (30). For bispheres, it is used with characteristics bounded in $d_1,d_2\in(0.1, 1)$ μm, $n\in[1.38, 1.6]$, $\beta\in[0°, 90°]$.

Both applied algorithms not only find best-fit model characteristics by minimization of $S(\mathbf{P})$ but also calculate their mathematical expectations and estimate the uncertainties based on Bayesian method (30,36). Moreover, the latter adequately responds (by larger errors of characteristics) to model deviations, for example, when nonspherical particle is fitted by a spherical model (36). Applying both models to each MP, we chose the best model on a single-particle basis using the Bayesian information criterion (45).

Results

Identification and Characterization of PLTs and MPs in PRP

At the first stage, we studied the untreated PRP. The reference 1-μm polystyrene beads added to each sample are clearly visible in SSC × FSC maps (Figs. 2B1 and 2B2). They are defined by gate L1 and removed from further consideration. As separation of PLTs and MPs is ambiguous in terms of SSC and FSC, we separate PLTs from MPs as described in subsection "Platelet and MP identification in PRP." The result of the first stage is shown in Figure 2A1 (1,600 events), where

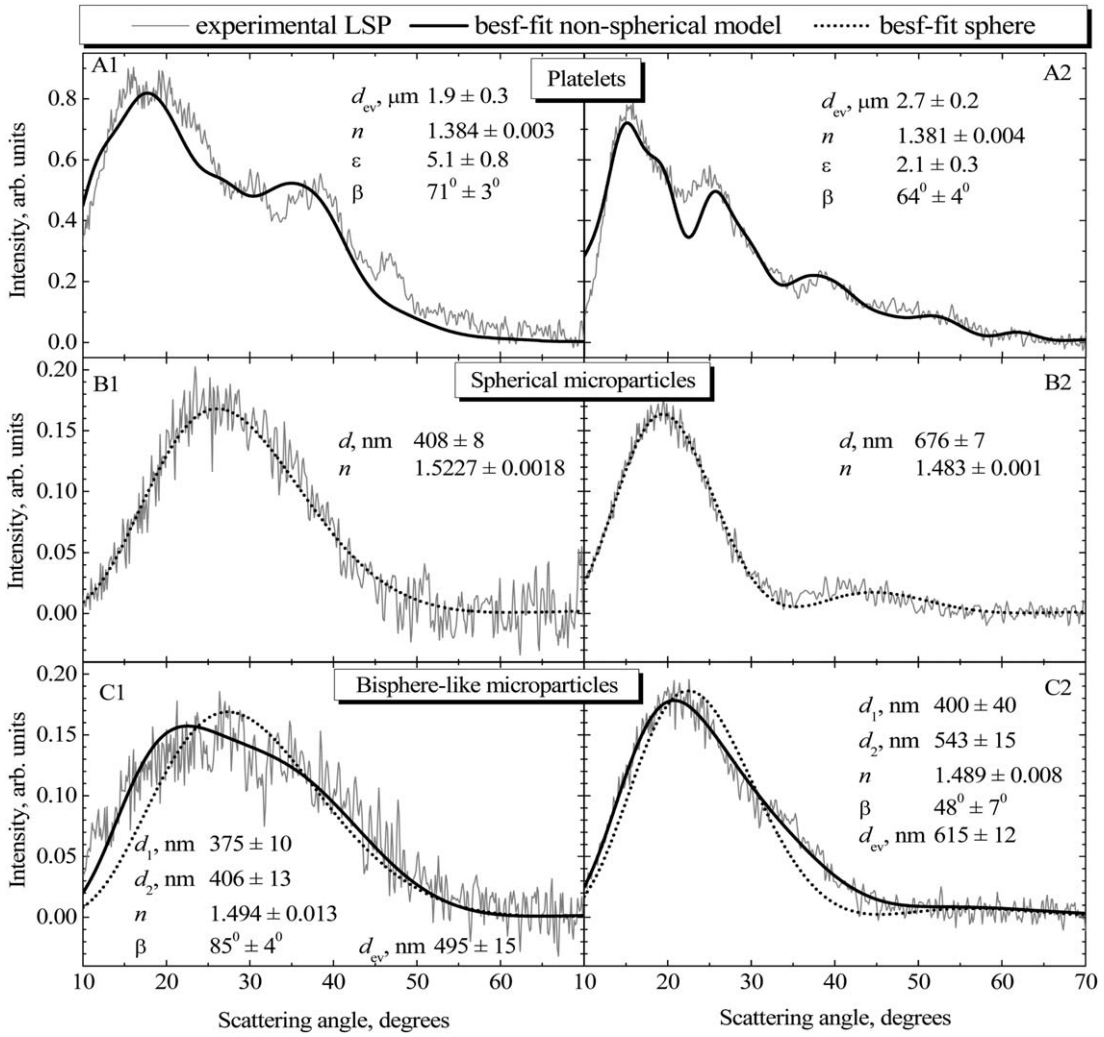

Figure 3. Typical results of the solution of the ILS problem for experimental LSPs of PLTs and MPs, depicting weighted experimental and best-fit theoretical LSPs (based on spherical or nonspherical model). Estimates of model characteristics are also shown (mathematical expectation ± standard deviation), including diameters d (or equivolume one d_{ev}), RI n, orientation angle β, and platelet aspect ratio ε. For bisphere-like MPs, the best-fit spherical LSPs are also shown to demonstrate the advantage of the bisphere model.

particles inside the PLT gate constitute 95% of all events. At the second stage, we studied centrifuged PRP. Figure 2A2 (3,000 events) shows that centrifugation removed larger PLTs resulting in a decrease of the fraction of events inside the PLT gate (76% of all events). We note that the diameters of remaining (non-PLT) particles defined at this stage (in contrast to that described later) are largely biased due to the use of PLT-oriented database.

Particles outside of the PLT gate are further processed as described in subsection "ILS problem" and are separated into three fractions: 1) well modeled by a sphere, 2) well modeled by a bisphere, and 3) not-identified particles. First, the bispheres are identified according to the model comparison criterion. The remaining particles are better described by a sphere, but only part of them has sufficiently small uncertainties of their characteristics. For the remaining part (labeled as not-identified particles), large uncertainties indicate that spherical model is also not suitable. Specifically, the separation between the latter two classes is performed based on relative errors of size (data not shown). We suppose that not-identified particles correspond to a larger MPs aggregates or some other plasma constituents. In particular, such aggregates were previously detected by other methods, such as confocal and electron microscopy (46,47). The FSC versus true MP diameters (d or d_{ev}) are separately shown in the inset in Figure 2A2. To contrast our algorithm with capabilities of the conventional flow cytometry in MP identification, we demonstrate the ordinary FSC versus SSC maps for the same samples in Figures 2B1 and 2B2. The 0.4-μm polystyrene beads are also shown for a reference. PLTs and MPs overlap to a larger extent in these maps. Moreover, FSC of 0.4-μm beads and MP events are grossly overlapping, although SSC allows one to discriminate between them. Still, part of PLTs fall into this range of smaller SSC. In general, there are no simple relations between FSC or SSC intensities and particle characteristics. Moreover, these quantities depend on a specific instrument.

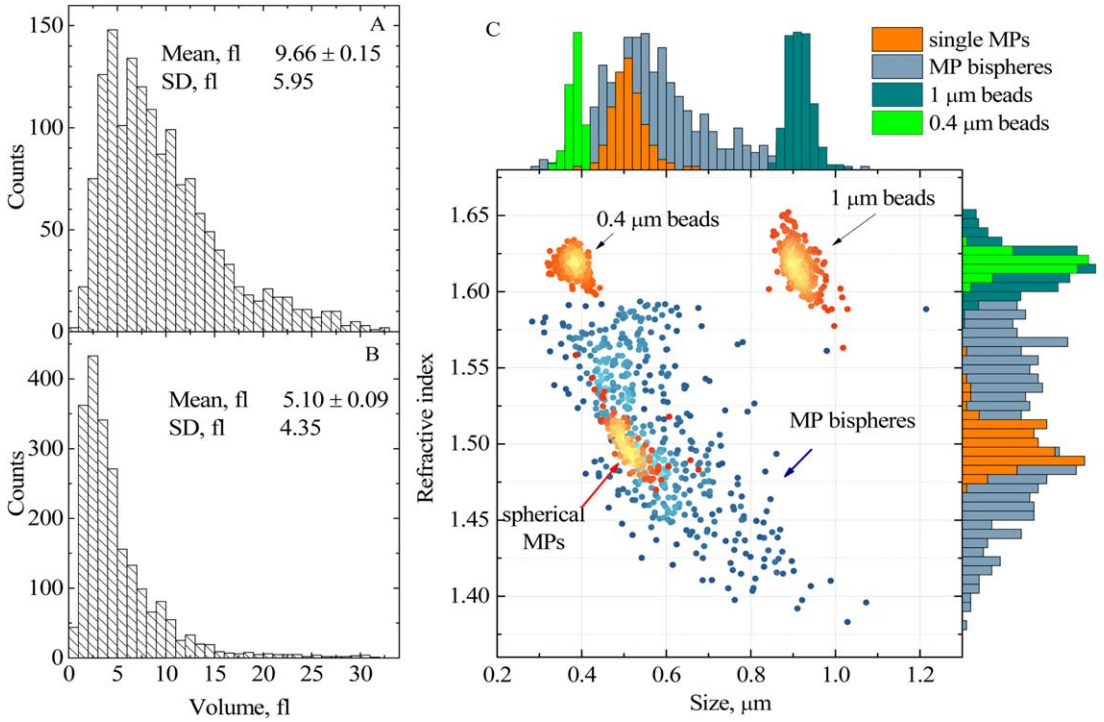

Figure 4. The characterization of the plasma particles. The platelet volume distribution for untreated (**A**) and centrifuged (**B**) PRP. Dot-density diameter versus RI map with corresponding distributions for MPs (**C**). The 1-μm and 0.4-μm polymer beads are shown for a reference. [Color figure can be viewed in the online issue, which is available at wileyonlinelibrary.com.]

For instance, the FSC signal in ordinary flow cytometers is formed by two components: scattering over the open aperture and diffraction of near-zero-angle light scattering on the beam stop, both of which are instrument-specific. Thus, we confirm that polystyrene beads are not suitable as universal optical standards for identification of a MP on FSC versus SSC map (13,28,29).

Typical results of single-particle characterization (solution of the ILS problem) for PLTs, spherical, and bisphere-like MPs are shown in Figures 3A1, 3A2, 3B1, 3B2, 3C1, and 3C2, respectively, depicting experimental LSPs, best-fit theoretical simulations, and determined particle characteristics together with uncertainties. We emphasize high precision in determination of the size and RI of spherical particles from the LSP and SSC measured with the SFC. The particle distributions and corresponding parameters are shown in Figure 4 and Table 1, respectively. The characterization results for PLTs are provided in Figures 4A and 4B by distributions over PLT volume in untreated and centrifuged PRP, respectively. The former distribution (Fig. 4A) is typical for blood PLTs, while the latter has predictably smaller right-hand tail (Fig. 4B).

To be independent on an optical setup of a particular flow cytometer in analysis of MPs, one should analyze the real MP characteristics, that is, construct the RI versus size map instead of FSC versus SSC map. We constructed such maps for single spherical MPs, bispheres, and 0.4- and 1-μm polystyrene beads and present them in Figure 4C. The beads and MPs can be easily separated from each other. Moreover, RI of beads agrees with the literature data for polystyrene (48). The developed method and current setup of the SFC allowed us to reliably characterize the fraction of single spherical MPs, which falls in the range of 450–600 nm for size and 1.48–1.52 for RI, as demonstrated by 1D distributions over particle characteristics in Figure 4. The distributions of bispheres are broader than that of spherical MPs due to the larger uncertainties in determination of their characteristics caused by their more complex model. Nonetheless, d_{ev} of bispheres falls in the range of 300–1,000 nm, and the majority of them have RI close to that of spherical MPs, so, we conclude that these bispheres primarily consist of the same relatively dense MPs. We also note the unprecedented precision of spherical MP characterization by a flow system. In particular, the median SDs of MP size and RI are 6 nm and 0.003, respectively, (Table 1), which can be contrasted to 45 nm and 0.016, respectively, in the previous study (31).

Characterization of MPs in Filtered PRP

The result for the filtered PRP is shown in Figure 5A (1,800 events). The filtration removed most of PLTs so the remaining part (inside the PLT gate) constituted only 10% of all events. As we mentioned earlier, the filtration may lead to PLT activation and fragmentation increasing MP counts. Distribution over MP characteristics is presented in RI versus size map (Fig. 5B). There are no substantial differences in the fraction of dense spherical MPs in comparison to centrifuged plasma sample, but bisphere characteristics are significantly changed. Unfortunately, the current setup does not allow us to detect spherical MPs of lower density (as their SSC is below

Table 1. Characteristics of the microparticles, polymer beads, and platelets retrieved by solving the inverse light-scattering problem

	PLATELETS		MICROPARTICLES						
			CENTRIFUGED PLASMA			FILTERED PLASMA			
CHARACTERISTICS	UNTREATED PLASMA	CENTRIFUGED PLASMA	SPHERICAL	BISPHERE-LIKE		SPHERICAL	BISPHERE-LIKE	1-μm BEADS	0.4-μm BEADS
Mean size (nm)	2536 ± 13	2010 ± 11	511 ± 3	578 ± 6		502 ± 5	600 ± 3	915.7 ± 0.7	384.3 ± 0.8
SD (nm)	525	501	41	132		46	120	26	18
Median (nm)	2,509	1,926	507	554		501	585	914	386
Mean refractive index	1.3816[a]	1.3808[a]	1.4994 ± 0.0012	1.507 ± 0.002		1.5053 ± 0.0016	1.4612 ± 0.0012	1.6163 ± 0.0007	1.6184 ± 0.0002
SD	0.003[a]	0.003[a]	0.0143	0.049		0.0159	0.0416	0.0123	0.0058
Median	1.3817[a]	1.3809[a]	1.4966	1.503		1.5018	1.459	1.6163	1.6186
Median uncertainty (SD) of size (nm)	345	247	6	30		5	36	19	8
Median uncertainty (SD) of RI			0.003	0.017		0.003	0.014	0.005	0.0016
Particles in sample (%)	95	75.5	4.7	16.1		5.2	72.6		

Mean values are accompanied (±) by standard errors of mean.
[a]The values of RI for platelets are not informative, as it is a priori constraint in the narrow range for the platelet-processing algorithm (30).

the detection threshold). However, we can observe their increment indirectly through the increased fraction of bispheres with lower RI, which were not present in the PRP. The difference in MP RI may correspond to different classes of MPs, which could be discriminated by size, protein components, protein/lipid ratio, and their functional activity (49). MPs with a higher protein/lipid ratio would have higher RI, whereas MPs containing only cytosol would have RI close to 1.38–1.41. Thus, increased fraction of lower density MPs is expected after filtration.

The amount of the MPs is increased from centrifuged to filtered PRP, mostly due to larger amount of bisphere-like MPs and not-identified particles. The fraction of the latter is about 15% of all particles outside the PLT gate in both cases. As noted above, not-identified particles may be attributed to larger MP aggregates or MP of other complex shapes. Moreover, part of them may be attributed to small activated PLTs with pseudopodia, which are well described neither by the PLT database nor by any of the MP shape model. Therefore, we consider the analysis of unfiltered PRP to be more accurate despite an increase in measuring time to collect sufficient number of MPs for characterization. Moreover, the separation of PLTs from other particles on FSC versus SSC map is even more ambiguous for the filtered sample (data not shown) than that for the centrifuged one (Fig. 2B2).

The parameters of distributions of all studied particles over their characteristics are presented in Table 1. We note that the utilization of the SSC amplitude in the solution of the ILS problem also increases the precision in sizing and RI determination of all spherical particles, including polystyrene beads. This is especially illustrative for 0.4-μm beads, for which median single-particle characterization uncertainties (SD) of size and RI is 8 nm and 0.0016, respectively, (Table 1). This is better than the best precision achieved previously with the SFC (34), where median uncertainties for 2-μm beads were 12 nm and 0.006, respectively. Precision of spherical-MP characterization is also very good (similar to that of 0.4-μm beads). In particular, this allows reliable discrimination of two MP fractions based on their RI (density).

Discussion

This article describes the second step in development of the method for identification and characterization of individual MPs using an angle-resolved light scattering measured with the inventive flow cytometer. As the fundamental problem of identification of MPs has been solved previously (31), this work is focused on improving the accuracy of both identification and characterization algorithms. Both challenges were solved using laser of 405 nm wavelength (the shortest in the visible band) and extra light-scattering data, the SSC amplitude that was added to the LSP in the inversion procedure. The developed two-stage algorithm has allowed us to perform label-free identification of cell-derived MPs among other particles in the PRP and characterize MPs solely from light scattering. Simultaneously, we characterized the PLTs with subdiffraction precision.

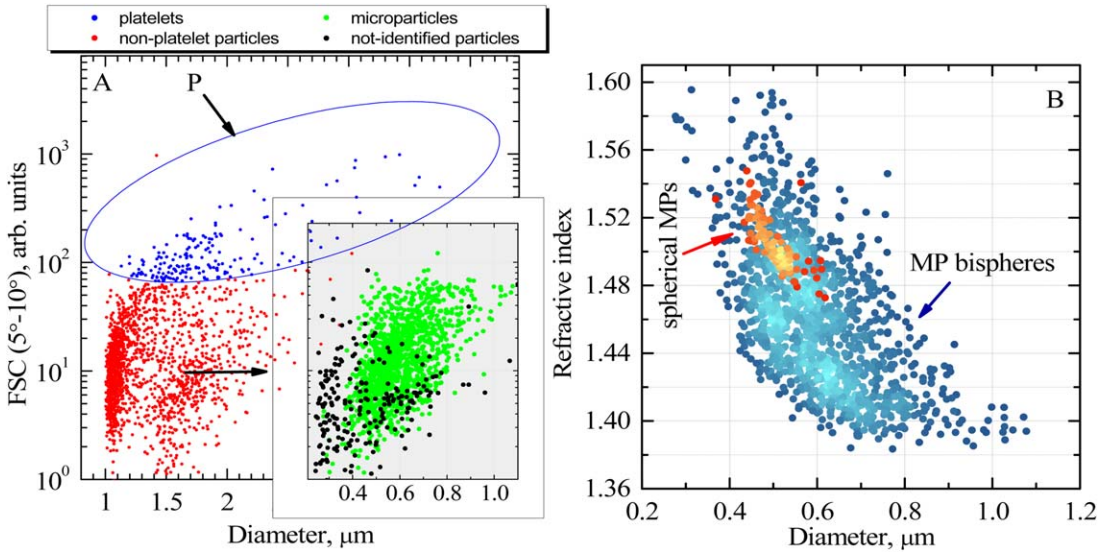

Figure 5. (**A**) FSC versus equivolume diameter scattering map of filtered PRP. The processing is the same as in Figure 2A2. (**B**) Dot-density diameter versus RI map of the corresponding MPs, which are colored green in (A). [Color figure can be viewed in the online issue, which is available at wileyonlinelibrary.com.]

Let us further estimate the detection limit for MP analysis from light scattering. Following Figure 4C, we conclude that the current optical setup of the SFC is suitable for analysis of MPs larger than 400 and 450 nm for more and less dense (in terms of RI) fractions of MPs, respectively. Theoretically, replacing the 488 nm laser, generating the SSC signal, with a 405 nm one will drop down the detection limit to 250 and 400 nm, respectively. It can be further decreased to 100 and 150 nm, respectively, using high-power lasers and middle-angle scattering instead of SSC. However, we are not expecting the high precision in characterization of MPs smaller than 150 nm because the structure of LSP is featureless for such MPs, making it very hard to determine both size and RI independently.

Despite the limitations of size of detectable MP, at present, the method allows one to identify MPs among PLTs in PRP and to determine their size with nanometer precision and RI with a precision of a few thousands. This leads to the instrument-independent quantitative characterization of MP as RI versus size map or 1D distributions over those characteristics. Such measurements would be useful in studies of cellular sources of MPs under different treatments, as the treatment is expected to change the statistical parameters of the distribution like mean, standard deviation, median, and so forth. In addition, the method is capable of detecting features in MP size (or RI) distributions, such as multipeak structure. In particular, we detected two classes of MP in filtered PRP based on their RI, which presumably correspond to different origin of these MPs.

Literature Cited

1. Burnier L, Fontana P, Kwak BR, Angelillo-Scherrer A. Cell-derived microparticles in haemostasis and vascular medicine. Thromb Haemost 2009;101:439–451.
2. Freyssinet J-M, Toti F. Formation of procoagulant microparticles and properties. Thromb Res 2010;125(Suppl 1):S46–S48.
3. Piccin A, Murphy WG, Smith OP. Circulating microparticles: Pathophysiology and clinical implications. Blood Rev 2007;21:157–171.
4. Ratajczak J, Wysoczynski M, Hayek F, Janowska-Wieczorek A, Ratajczak MZ. Membrane-derived microvesicles: Important and underappreciated mediators of cell-to-cell communication. Leukemia 2006;20:1487–1495.
5. Enjeti AK, Lincz LF, Seldon M. Microparticles in health and disease. Semin Thromb Hemost 2008;34:683–691.
6. Mause SF, Weber C. Microparticles protagonists of a novel communication network for intercellular information exchange. Circ Res 2010;107:1047–1057.
7. Ayers L, Kohler M, Harrison P, Sargent I, Dragovic R, Schaap M, Nieuwland R, Brooks SA, Ferry B. Measurement of circulating cell-derived microparticles by flow cytometry: Sources of variability within the assay. Thromb Res 2011;127:370–377.
8. Barteneva NS, Fasler-Kan E, Bernimoulin M, Stern JN, Ponomarev ED, Duckett L, Vorobjev IA. Circulating microparticles: Square the circle. BMC Cell Biol 2013;14:23.
9. Chandler WL. Microparticle counts in platelet-rich and platelet-free plasma, effect of centrifugation and sample-processing protocols. Blood Coagul Fibrinolysis 2013;24:125–132.
10. Bohling SD, Pagano MB, Stitzel MR, Ferrell C, Yeung W, Chandler WL. Comparison of clot-based vs chromogenic factor Xa procoagulant phospholipid activity assays. Am J Clin Pathol 2012;137:185–192.
11. Dinkla S, Brock R, Joosten I, Bosman GJ. Gateway to understanding microparticles: Standardized isolation and identification of plasma membrane-derived vesicles. Nanomedicine 2013;8:1657–1668.
12. Horstman LL, Ahn YS. Platelet microparticles: A wide-angle perspective. Crit Rev Oncol Hematol 1999;30:111–142.
13. Chandler WL, Yeung W, Tait JF. A new microparticle size calibration standard for use in measuring smaller microparticles using a new flow cytometer. J Thromb Haemost 2011;9:1216–1224.
14. Shapiro HM. Practical Flow Cytometry, 4th ed. New York: Wiley-Liss; 2003. 736 p.
15. Wedd MW. Determination of particle size distributions using laser diffraction. Educ Resour Part Technol 2003;4:1–4.
16. Hurley J. Sizing particles with a coulter counter. Biophys J 1970;10:74–79.
17. Sun T, Morgan H. Single-cell microfluidic impedance cytometry: A review. Microfluid Nanofluid 2010;8:423–443.
18. Xu Y, Nakane N, Maurer-Spurej E. Novel test for microparticles in platelet-rich plasma and platelet concentrates using dynamic light scattering. Transfusion 2011;51:363–370.
19. Lawrie AS, Albanyan A, Cardigan RA, Mackie IJ, Harrison P. Microparticle sizing by dynamic light scattering in fresh-frozen plasma. Vox Sang 2009;96:206–212.
20. Anderson W, Kozak D, Coleman VA, Jämting ÅK, Trau M. A comparative study of submicron particle sizing platforms: Accuracy, precision and resolution analysis of polydisperse particle size distributions. J Colloid Interface Sci 2013;405:322–330.
21. Van der Pol E, Hoekstra AG, Sturk A, Otto C, van Leeuwen TG, Nieuwland R. Optical and non-optical methods for detection and characterization of microparticles and exosomes. J Thromb Haemost 2010;8:2596–2607.
22. Yuana Y, Bertina RM, Osanto S. Pre-analytical and analytical issues in the analysis of blood microparticles. Thromb Haemost 2011;105:396–408.
23. Dragovic RA, Gardiner C, Brooks AS, Tannetta DS, Ferguson DJP, Hole P, Carr B, Redman CWG, Harris AL, Dobson PJ, et al. Sizing and phenotyping of cellular vesicles using nanoparticle tracking analysis. Nanomedicine 2011;7:780–788.

24. Van der Pol E, Coumans FAW, Sturk A, Nieuwland R, van Leeuwen TG. Refractive index determination of nanoparticles in suspension using nanoparticle tracking analysis. Nano Lett 2014;14:6195–6201.
25. Lacroix R, Robert S, Poncelet P, Kasthuri RS, Key NS, Dignat-George F, Workshop OB of the IS. Standardization of platelet-derived microparticle enumeration by flow cytometry with calibrated beads: Results of the International Society on Thrombosis and Haemostasis SSC Collaborative workshop. J Thromb Haemost 2010;8:2571–2574.
26. Mullier F, Bailly N, Chatelain C, Dogné JM, Chatelain B. More on: Calibration for the measurement of microparticles: Needs, interests, and limitations of calibrated polystyrene beads for flow cytometry-based quantification of biological microparticles. J Thromb Haemost 2011;9:1679–1681.
27. Robert S, Poncelet P, Lacroix R, Raoult D, Dignat-George F. More on: Calibration for the measurement of microparticles: Value of calibrated polystyrene beads for flow cytometry-based sizing of biological microparticles. J Thromb Haemost 2011;9:1676–1678.
28. Nolan JP, Stoner SA. A trigger channel threshold artifact in nanoparticle analysis. Cytometry Part A 2013;83A:301–305.
29. Van der Pol E, van Gemert MJC, Sturk A, Nieuwland R, van Leeuwen TG. Single vs. swarm detection of microparticles and exosomes by flow cytometry. J Thromb Haemost 2012;10:919–930.
30. Moskalensky AE, Yurkin MA, Konokhova AI, Strokotov DI, Nekrasov VM, Chernyshev AV, Tsvetovskaya GA, Chikova ED, Maltsev VP. Accurate measurement of volume and shape of resting and activated blood platelets from light scattering. J Biomed Opt 2013;18:017001.
31. Konokhova AI, Yurkin MA, Moskalensky AE, Chernyshev AV, Tsvetovskaya GA, Chikova ED, Maltsev VP. Light-scattering flow cytometry for identification and characterization of blood microparticles. J Biomed Opt 2012;17:057006.
32. Maltsev VP, Chernyshev AV, Strokotov DI. Light-scattering flow cytometry: Advanced characterization of individual particle morphology. In: Papandreou S, editor. Flow Cytometry: Principles, Methodology and Applications. New York, NY: Nova Science Publishers; 2013. pp 79−103.
33. Maltsev VP. Scanning flow cytometry for individual particle analysis. Rev Sci Instrum 2000;71:243–255.
34. Strokotov DI, Moskalensky AE, Nekrasov VM, Maltsev VP. Polarized light-scattering profile—advanced characterization of nonspherical particles with scanning flow cytometry. Cytometry Part A 2011;79A:570–579.
35. Bohren CF, Huffman DR. Absorption and Scattering of Light by Small Particles, 1st ed. New York: Wiley; 1983. 544 p.
36. Strokotov DI, Yurkin MA, Gilev KV, van Bockstaele DR, Hoekstra AG, Rubtsov NB, Maltsev VP. Is there a difference between T- and B-lymphocyte morphology? J Biomed Opt 2009;14:064036.
37. Yurkin MA, Hoekstra AG. The discrete-dipole-approximation code ADDA: Capabilities and known limitations. J Quant Spectrosc Radiat Transf 2011;112:2234–2247.
38. Rousseeuw PJ, Driessen KV. A fast algorithm for the minimum covariance determinant estimator. Technometrics 1998;41:212–223.
39. Todorov V, Filzmoser P. An object oriented framework for robust multivariate analysis. J Stat Softw 2009;32:1–47.
40. Junkar I, Šuštar V, Frank M, Janša V, Bedina Zavec A, Rozman B, Mozetič M, Hägerstrand H, Kralj-Iglič V. Blood and synovial microparticles as revealed by atomic force and scanning electron microscope. Open Autoimmun J 2009;1:e50–e58.
41. György B, Módos K, Pállinger É, Pálóczi K, Pásztói M, Misják P, Deli MA, Sipos Á, Szalai A, Voszka I, et al. Detection and isolation of cell-derived microparticles are compromised by protein complexes resulting from shared biophysical parameters. Blood 2011;117:e39–e48.
42. Mishchenko MI, Travis LD. Capabilities and limitations of a current FORTRAN implementation of the T-matrix method for randomly oriented, rotationally symmetric scatterers. J Quant Spectrosc Radiat Transf 1998;60:309–324.
43. Xu S, Liu J, Sun Z. Optical factors determined by the T-matrix method in turbidity measurement of absolute coagulation rate constants. J Colloid Interface Sci 2006;304:107–114.
44. Jones DR, Perttunen CD, Stuckman BE. Lipschitzian optimization without the Lipschitz constant. J Optim Theory Appl 1993;79:157–181.
45. Schwarz G. Estimating the dimension of a model. Ann Stat 1978;6:461–464.
46. Hughes M, Hayward CP, Warkentin TE, Horsewood P, Chorneyko KA, Kelton JG. Morphological analysis of microparticle generation in heparin-induced thrombocytopenia. Blood 2000;96:188–194.
47. Peramo A, Diaz JA. Physical characterization of mouse deep vein thrombosis derived microparticles by differential filtration with nanopore filters. Membranes 2011;2:1–15.
48. Kasarova SN, Sultanova NG, Ivanov CD, Nikolov ID. Analysis of the dispersion of optical plastic materials. Opt Mater 2007;29:1481–1490.
49. Dean WL, Lee MJ, Cummins TD, Schultz DJ, Powell DW. Proteomic and functional characterisation of platelet microparticle size classes. Thromb Haemost 2009;102:711–718.